

Comparative Numerical Study of Pulse Tube Refrigerators

T.R Ashwin, G.S.V.L Narasimham and S. Jacob

Indian Institute of Science
Bangalore, India 560012.

ABSTRACT

The focus of this work is the modeling and performance comparison of different models of pulse tube refrigerators, namely, the Orifice Pulse Tube Refrigerator (OPTR) and the Inertance-tube Pulse Tube Refrigerator (IPTR) with both in-line as well as coaxial configurations. A detailed analysis of the flow and heat transfer in various components of the above mentioned models under oscillating flow conditions is carried out using FLUENT. Parametric studies are also performed with different length-to-diameter ratios of the IPTR in-line design, in order to determine the optimum geometry for attaining the lowest temperature in the cold heat exchanger under no-load condition. The components of the OPTR are the compressor, transfer line, after cooler, regenerator, cold heat exchanger, pulse tube, hot heat exchanger, orifice valve (usually a needle valve to control the mass flow rate) and the buffer. The modeling of IPTR requires the modeling of inertance tube (a long narrow tube) instead of orifice. The mathematical model consists of the full set of compressible conservation equations with the assumption of axi-symmetry. The regenerator and other heat exchangers are modeled using porous approximation both with thermal equilibrium and thermal non-equilibrium assumption. The effect of axial conduction on performance of pulse tube refrigerator is also analyzed by introducing the wall thickness. The results show that the no-load temperature reached in the cold heat exchanger of IPTR in-line configuration is lower compared to other models. It can also be seen that the interaction of the pulse tube wall and the oscillating flow is an important factor, and that the simplified models tend to over-predict the cold heat exchanger temperature. The thermal non-equilibrium analysis yields a lower cold heat exchanger temperature.

INTRODUCTION

The discovery of the basic pulse tube refrigerator was made by Gifford and Longworth¹ as early as 1960's. One major design modification for performance improvement led to the development of Orifice Pulse Tube Refrigerator (OPTR). In an Inertance Pulse Tube Refrigerator (IPTR) (Figure 1), an inertance tube, which is simply a long and narrow tube, replaces the orifice valve of the OPTR. The inertance tube imposes a hydraulic resistance and an inductance to the flow. By varying the dimensions of the inertance tube, an adjustable delay between the pressure responses of the pulse tube and the reservoir can be created. In the recent past, pulse tube coolers are being increasingly favored for cryocoolers because of its simplicity and the absence of moving parts in the low temperature region of the refrigerator.

The mechanism of energy transfer in a PTR is not fully understood despite concerted efforts of researchers. A one-dimensional numerical model for IPTR and thermoacoustic refrigerator was

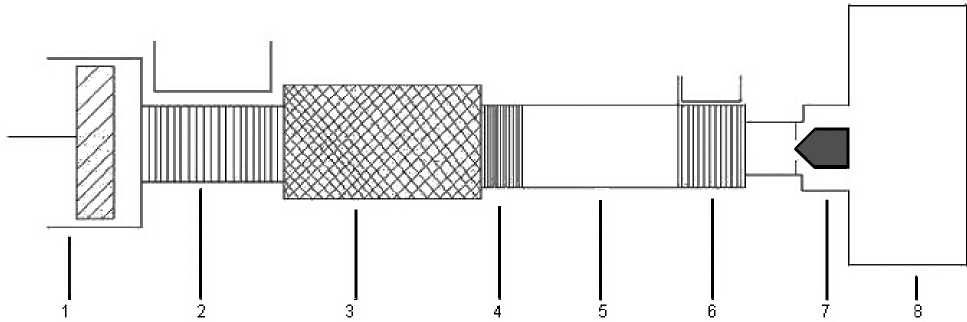


Figure 1. Integrated Model of an inline Orifice Pulse Tube Refrigerator (1) Compressor, (2) After cooler, (3) Regenerator, (4) Cold heat exchanger, (5) Pulse Tube, (6) Hot heat exchanger (7) Orifice (8) Buffer.

developed by Zhu et al.¹ The phase lag between pressure and mass flow is an important factor influencing the performance of IPTR². Cha et al.³ carried out analysis of a high frequency miniature PTR using the CFD (Computational Fluid Dynamics) package FLUENT®. Flake and Razani⁴ also used CFD as a tool to simulate the performance of OPTR with an axis-symmetric model, and studied the recirculation pattern and streaming in a PTR with the help of FLUENT®. The aforementioned models used thermal equilibrium assumption for the porous zones (regenerator and the heat exchangers) in the PTR. However, Harvey⁵ accounted for the non-thermal equilibrium between the working fluid and the solid matrix using a one-dimensional formulation.

Tanaka et al.⁶ investigated the heat transfer characteristics of a regenerator with oscillating flow. Imura et al.⁷ tested the characteristics of a regenerator for various mesh numbers under high oscillating frequency conditions. Koh and Fortini⁸, developed an empirical correlation for stainless steel wire mesh screens. Most recently, Clearman et al.⁹ experimentally measured and correlated the hydrodynamic parameters associated with the flow of helium in regenerator fillers.

The objective of the present work is the complete CFD analysis of OPTR and IPTR with in-line and coaxial configurations. Parametric studies are conducted on an IPTR in-line configuration with different length-to-diameter ratios of the pulse tube. These studies mainly concentrate on finding an optimum geometry for the lowest cold heat exchanger temperature. The oscillating axis-symmetric flow and temperature fields in the various components of pulse tubes are computed by solving the full set of compressible flow conservation equations. The porous zones are modeled taking into account the more realistic thermal non-equilibrium between the gas and the matrix. A comparative study is also made between the thermal equilibrium and thermal non-equilibrium models. The effect of axial conduction on performance of pulse tube refrigerators is analyzed by comparing the performance of models with and without wall thickness.

PTR CONFIGURATION

Figure 2 shows the miniature pulse tube model with individual components. The integrated model consists of compressor (1), transfer line (2), compressor cooler (3), regenerator (4), cold heat exchanger (5), pulse tube (6), hot heat exchanger (7) inertance tube for IPTR and Orifice for OPTR

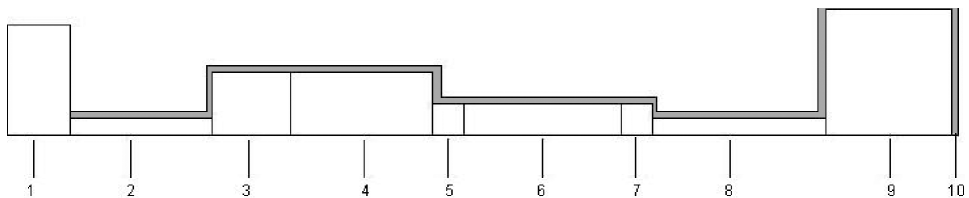


Figure 2. Schematic of inline inertance tube pulse tube refrigerator with finite wall thickness

(8) buffer (9) and the component wall (10). The finite thickness of the wall material of the various components is also taken into account as shown in Figure 2. The wall material for various components of the pulse tube refrigerator is as indicated in Table 1.

INITIAL AND BOUNDARY CONDITIONS

The swept volume of the compressor is 1.06 cm^3 and the clearance space is 0.17 cm^3 . The initial charge pressure is 25 bar at an ambient temperature of 300 K. The working fluid is helium and is assumed to obey the ideal gas equation. The walls of the compressor after-cooler and hot heat exchangers are maintained at ambient temperature. Perfect cooling is assumed in the compressor after-cooler. The cold heat exchanger wall is maintained at adiabatic condition (i.e., no load) as also the other walls of the system.

Parametric Studies Parametric studies are conducted on five different models of length-to-diameter ratio of 4.28, 12.5, 18.75, 25 and 37.5 respectively for a pulse tube diameter of 4 mm. The geometrical details and boundary conditions are listed in detail in Table 1. The pulse tube diameters of the above models are kept constant at 4 mm and the length is varied.

Comparative Studies of Different Types Other than parametric studies, some runs are taken for comparing the performance of OPTR, IPTR with coaxial and in-line configuration. This is done with models of length-to-diameter ratio of 25 and buffer length of 40 mm. Other geometrical dimensions and boundary conditions are the same as in Table 1. Three different coaxial designs with inertance tube lengths of 150 mm, 300 mm and 500 mm have been studied. The volume of each component is kept the same for all the types for comparison purpose.

MODELING DETAILS

Mesh Generation The modeling of the geometry and nodalization of various parts are done using GAMBIT®. The junction regions of the components are represented with finer meshes for better numerical resolution. The number of grid points varies between 4500 and 7200 for different models.

Modeling of Compressor Dynamic meshing is used to model the compressor in which the volume of the domain changes with time. A User Defined Function (UDF) is written to track and properly guide the motion of the compressor piston with respect to time. The updating of the mesh is automatically done by FLUENT at each time step, depending upon the new position of the piston. Various dynamic meshing methods like “dynamic-layering”, “remeshing” and “spring based smoothing” are used for updating the meshing in the deforming volume. The operating frequency f is chosen as 50 Hz and the angular velocity is $\omega = 2\pi f$. The piston movement is traced by the relation, $L = L_0 \sin(\omega t)$ where $L_0 = 3 \times 10^{-3} \text{ mm}$ is the amplitude.

Modeling of Porous Zones The flow losses are determined by choosing appropriate values for inertial resistance, permeability and porosity. For the porous zones, appropriate modeling is used by considering extra momentum sink terms in the momentum equations and the energy source or sink terms in the fluid and matrix energy equations.

Table 1. Geometry details and Boundary Conditions*

Component Name	Diameter	Length	Wall thickness	Wall Material	Boundary Condition
Compressor Piston (1)	15	6			Adiabatic
Transfer Line (2)	2	100	0.3	SS-304	Adiabatic
Compressor cooler (3)	6	16	0.3	OFHC-Cu	300K
Regenerator (4)	6	60	0.3	SS-304	Adiabatic
Cold heat exchanger (5)	4	4	1	OFHC-Cu	Adiabatic
Pulse Tube (6)	4	30	0.3	Titanium	Adiabatic
Hot heat exchanger (7)	4	15	0.3	OFHC-Cu	300K
Inertance tube (8)	0.6	300	0.3	SS-304	Adiabatic
Buffer (9)	30	80	0.3	SS-304	Adiabatic

* All dimensions in mm

CALCULATION OF OTHER PARAMETERS

Calculation of Wire Mesh Parameters The heat exchangers, namely, the compressor cooler, cold heat exchanger and the hot heat exchanger are taken to be porous media with a wire mesh number 325, permeability $1.06 \times 10^{-10} \text{ m}^2$ and an inertial resistance of 76090 m^{-1} (Harvey⁵). The matrix material is stainless steel for the regenerator and OFHC-Cu for other heat exchangers. For wire mesh screen matrices, if d is the diameter of the wire and x_t is the transverse pitch of the wires, the porosity is given by $\phi = 1 - \pi/(4x_t)$. The transverse pitch multiplier is given by $x_t = 1/nd$, where n is the mesh number. The relations for the hydraulic radius r_h , porous cross-sectional area A_p and the transfer area A_t are $r_h = d[(x_t/\pi) - (1/4)]$, and $A_p = \phi A_{c,x}$. Where $A_{c,x}$ is the total cross-sectional area of the regenerator or the frontal area and L is the regenerator length. The equivalent diameter is $D_e = 4r_h$.

Calculation of Temperature-dependent Properties Viscosity, thermal conductivity and specific heat of the working gas and the solid matrixes are taken to be temperature-dependent. User Defined Functions (UDFs) for the calculation of variable thermophysical properties of the working medium and the porous matrixes are written and appropriately hooked to the FLUENT panel.

GOVERNING EQUATIONS

The governing equations, namely, the continuity, momentum and energy equations are written for a cylindrical coordinate system with the assumption of axi-symmetry and no swirl. The velocity components appearing in the equations are the superficial velocity components in the case of porous zones.

Continuity Equation
$$\frac{\partial}{\partial t}(\rho_f) + \frac{1}{r} \frac{\partial}{\partial r}(r \rho_f v_r) + \frac{\partial}{\partial z}(r \rho_f v_z) = 0 \quad (1)$$

Momentum Equation in Axial Direction

$$\frac{\partial}{\partial t}(\rho_f v_z) + \frac{1}{r} \frac{\partial}{\partial z}(r \rho_f v_z v_z) + \frac{1}{r} \frac{\partial}{\partial r}(r \rho_f v_r v_z) = -\frac{\partial p}{\partial z} + \frac{1}{r} \frac{\partial}{\partial z} \left[r \mu \left(2 \frac{\partial v_z}{\partial z} - 2 \left(\vec{\nabla} \bullet \vec{v} \right) \right) \right] + \frac{1}{r} \frac{\partial}{\partial r} \left[r \mu \left(\frac{\partial v_z}{\partial r} + \frac{\partial v_r}{\partial z} \right) \right] + S_z \quad (2)$$

Momentum Equation in Radial Direction

$$\frac{\partial}{\partial t}(\rho_f v_r) + \frac{1}{r} \frac{\partial}{\partial z}(r \rho_f v_z v_r) + \frac{1}{r} \frac{\partial}{\partial r}(r \rho_f v_r v_r) = -\frac{\partial p}{\partial r} + \frac{1}{r} \frac{\partial}{\partial z} \left[r \mu \left(\frac{\partial v_z}{\partial r} + \frac{\partial v_r}{\partial z} \right) \right] + \frac{1}{r} \frac{\partial}{\partial r} \left[r \mu \left(2 \frac{\partial v_r}{\partial r} - 2 \left(\vec{\nabla} \bullet \vec{v} \right) \right) \right] - 2 \mu \frac{v_r}{r^2} + \frac{2}{3} \mu \left(\vec{\nabla} \bullet \vec{v} \right) + S_R \quad (3)$$

The source terms are zero for nonporous zones. Separate axial and radial momentum source terms are included in the porous zones to account for the momentum losses. The resistance of the flow through the porous media is accounted by two terms, namely, the Darcy term in which the pressure drop is directly proportional to velocity and a Forchheimer term, in which the pressure drop is proportional to the square of the velocity. The solid matrix is assumed to be homogeneous. The momentum source terms in the porous zones in the axial and radial directions are respectively

$$S_z = - \left(\frac{\mu}{\beta} v_z + \frac{1}{2} C \rho_f |v| v_z \right) \text{ and } S_R = - \left(\frac{\mu}{\beta} v_r + \frac{1}{2} C \rho_f |v| v_r \right) \quad (4, 5)$$

Energy Equations for the gas and the matrix In describing the temperature distribution in a porous zone, the thermal equilibrium assumption is often invoked for simplifying the formulation. Under this assumption, the energy equation reads:

$$\frac{\partial}{\partial t}(\phi \rho_f E_f + (1 - \phi) \rho_s E_s) + \vec{\nabla} \bullet \left(\vec{v} (\rho_f E_f + p) \right) = \vec{\nabla} \bullet \left(k \vec{\nabla} T_f + \left(\tau \bullet \vec{v} \right) \right) \quad (6)$$

$$k = \phi k_f + (1 - \phi) k_s \quad \text{where} \quad E_f = \hat{h} - p / \rho_f + v^2 / 2 \quad (7)$$

In the thermal equilibrium model, the temperatures of the gas and solid structure are the same at any time and spatial location. Thus, in this model, the thermal interaction between the fluid and

the matrix is neglected by describing the temperature distribution with a single energy equation for the gas and matrix put together. However, in components like regenerators, where thermal inertia plays an important role, the consideration of non-thermal equilibrium tends to be more accurate. For non-thermal equilibrium model, separate energy equations are written for the matrix and the gas as follows:

Energy Equation for Matrix

$$\frac{\partial}{\partial t}(\rho_s E_s) = \vec{\nabla} \cdot \left(k_s \vec{\nabla} T_s \right) + S_s \quad (8)$$

i.e.

$$\frac{\partial}{\partial t}(\rho_s C_{p,s} T_s) = \frac{1}{r} \frac{\partial}{\partial r} \left[k_s r \frac{\partial T_s}{\partial r} \right] + \frac{\partial}{\partial z} \left[k_s \frac{\partial T_s}{\partial z} \right] + \frac{\alpha A_v (T_f - T_s)}{1 - \phi} \quad (9)$$

Energy Equation for Gas

$$\frac{\partial}{\partial t}(\rho_f E_f) + \vec{\nabla} \cdot \left(\vec{v} (\rho_f E_f + p) \right) = \vec{\nabla} \cdot \left(k \vec{\nabla} T_f + \left(\tau \bullet \vec{v} \right) \right) + S_G \quad (10)$$

For non porous zones, the energy source term S_θ is zero. However, in the porous zones, $S_g = \alpha A_v (T_s - T_f) / \phi$. Here α is the heat transfer coefficient between the gas and the matrix under oscillating flow conditions, A_v is the heat transfer area per unit volume of the zone, T_s is the matrix temperature and ϕ is the void fraction (or porosity).

Calculation of heat transfer coefficient between porous structure and the working gas For pulsating flow, heat transfer coefficient in the regenerator is given by Tanaka et.al.⁶

$$\alpha = 0.33 \frac{k_f}{D_e} \left(\frac{\rho_f D_e}{\mu} \frac{2 V_p \rho^*}{A_s \phi} \right)^{0.67} \quad (11)$$

Where $\rho^* = \rho_f (T_H) / \rho_f (T_{av})$. The quantities T_{av} and T_H are respectively the average temperature of the gas inside the regenerator and the hot end regenerator temperature.

Calculation of effective thermal conductivity of porous structure From Koh and Fortini⁹, the thermal conductivity of solid matrix can be obtained by neglecting the contribution of the helium gas. The resulting relation is

$$K_{eff} = \frac{1 - \phi}{1 + 11\phi} K_s \quad (12)$$

METHOD OF SOLUTION

The unsteady pressure based segregated solver with implicit formulation is used for solving the discretized equations. The first order method is used for unsteady terms as a compulsory option because of the dynamic meshing. The algorithm used is SIMPLE with suitable under-relaxation parameters to enhance the convergence. The solution of the equations is accomplished with the help of separate User Defined Scalars (UDSs) defined for each porous zone. The general scalar transport equation defined with the help of the UDSs contains four separate terms, namely, the unsteady term, convection term, diffusion term and the source term. These terms are properly customized and attached to the UDSs with the help of User defined Functions (UDFs). The absolute convergence criterion is 0.001 for the continuity, radial and axial velocities, and for the User Defined Scalars, while it is 10^{-6} for temperature. Preliminary numerical experimentation revealed that with the initial condition at room temperature (300 K), typically 500 seconds of real time is needed to reach an oscillatory state with a time step of 0.0005 seconds. At each time step, 50 inner iterations are used for proper coupling between the equations and for better convergence. It is observed that over 25 days of CPU is required for the system to reach a periodic state on a SUN workstation with 3 GHz processor and 2 GB of RAM.

RESULTS AND DISCUSSION

Temperature distributions of In-line OPTR, Coaxial IPTR and In-line IPTR Figure 3 shows the cyclic temperature variation of in-line OPTR and coaxial IPTR after reaching periodic state.

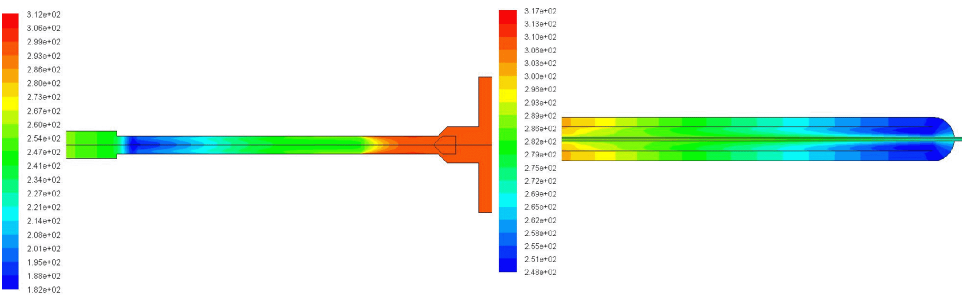


Figure 3. Temperature profile of inline OPTR and coaxial IPTR after reaching steady state.

The models assume with infinitesimally small wall thickness and thermal equilibrium of porous zones. It can be seen that the cold heat exchanger temperatures are 182 K and 203 K for in-line OPTR and coaxial IPTR respectively. In order to simplify the modeling and for the axis-symmetric condition, the inertance tube is taken out from the hot heat exchanger through cold heat exchanger along the axis and directly connected to the buffer. So there is rapid flow reversal in both cold as well as hot heat exchangers. This kind of rapid reversal introduced for modeling simplicity, is mainly responsible for the poor performance of coaxial IPTR. A good temperature gradient is established axially between the compressor cooler and the cold heat exchanger in both the cases. Figure 4a shows the axial temperature variation for in-line OPTR and in-line IPTR configurations after reaching a steady periodic condition. It may be recalled that perfect cooling is assumed in the compressor after cooler. Sharp temperature decrease and increase can be noticed in the in-line IPTR regenerator and the pulse tube. The variations observed in the in-line OPTR is more gradual compared to the in-line IPTR configuration. The in-line IPTR compressor is working at a higher temperature compared to the in-line OPTR. This shows that the resistance offered by inertance tube is much larger compared to orifice resulting in high temperature in the compressor region. The cold heat exchanger temperature is 110 K for in-line IPTR and 182 K for in-line OPTR. It can also be seen that the temperature decreases from the beginning to end of the cold and hot heat exchangers for both cases. The temperature variations in the inertance tube and the buffer are not significant for in-line IPTR. From Figure 4b, the in-line IPTR configuration with higher buffer volume of 56.54 cc is reaching lower cold heat exchanger temperature compared to the model with lower buffer volume of 28.27 cc. This shows that buffer volume has strong influence on cooldown characteristics.

Velocity Vector Plots. Figure 5a shows the velocity vector plots of an in-line OPTR at the entry to the compressor cooler. It can be seen that the two-dimensional effects are more prominent at the

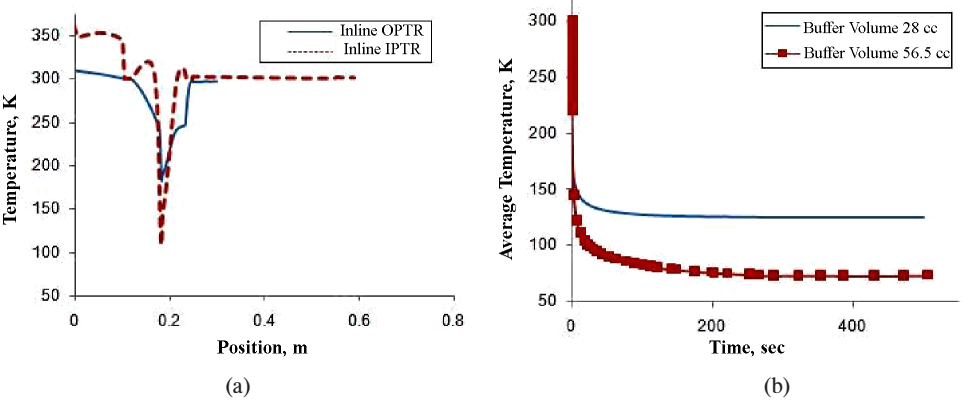


Figure 4. (a) Axial temperature variations for inline OPTR and IPTR configurations (b) Cooldown characteristics of inline IPTR with 28.27 cc and 56.5cc buffer volumes.

junctions between the components. Figure 5b shows that the velocity vector plots in the orifice region. There is a likelihood of eddy formation near the orifice at high velocities. This can adversely affect the performance of in-line OPTR compared to an in-line IPTR.

Pressure Profiles. Figures 6a and 6b show the pressure variation along the regenerator of an in-line IPTR with a length-to-diameter ratio of 25 with both thermal equilibrium and thermal non-equilibrium of porous zones after 1.005 seconds. In both the cases, pressure variation in the regenerator is almost one-dimensional. From Figure 6a, it can be noted that a pressure drop of about 1 bar is occurring in the regenerator.

Cooldown Characteristics. Figure 7a shows the cooldown characteristic of in-line OPTR, in-line IPTR and coaxial IPTR configurations. The results are obtained with models of infinitesimally small wall thickness and thermal equilibrium in the regenerator. It can be seen that the in-line IPTR performs better than other designs. The coaxial IPTR with 500 mm inertance tube length is reaches lower cold heat exchanger temperature compared to other coaxial models of lower inertance tube length. The characteristics associated with the rapid reversal of flow in the cold heat exchanger and hot heat exchanger is mainly responsible for the poor performance of coaxial IPTR compared to in-line models. Figure 7b shows the cyclic average temperature at the exit of the cold heat exchanger against the cooldown time for pulse tubes with different length-to-diameter ratio. These results are obtained for models with infinitesimally thin walls and thermal equilibrium assumption for the porous zones. The boundary and initial conditions are kept the same for comparison purpose. Pulse tubes with smaller length-to-diameter ratio are seen to stabilize at a higher cold heat exchanger

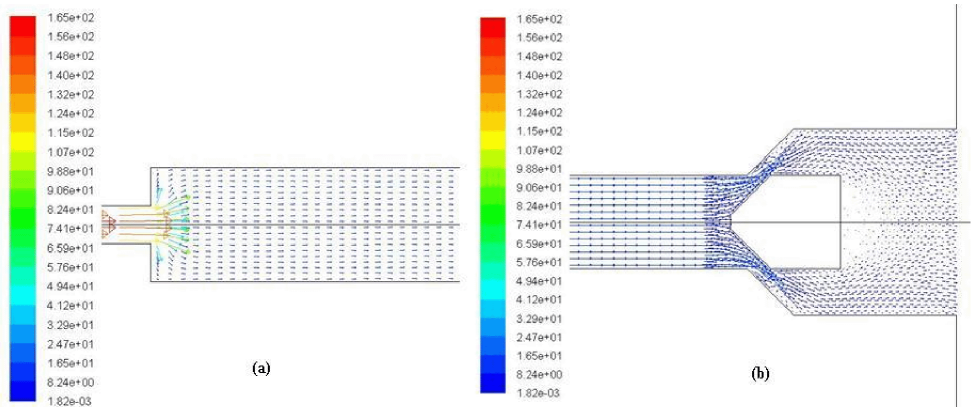


Figure 5. Velocity profile of inline OPTR at (a) Compressor Cooler (b) Orifice

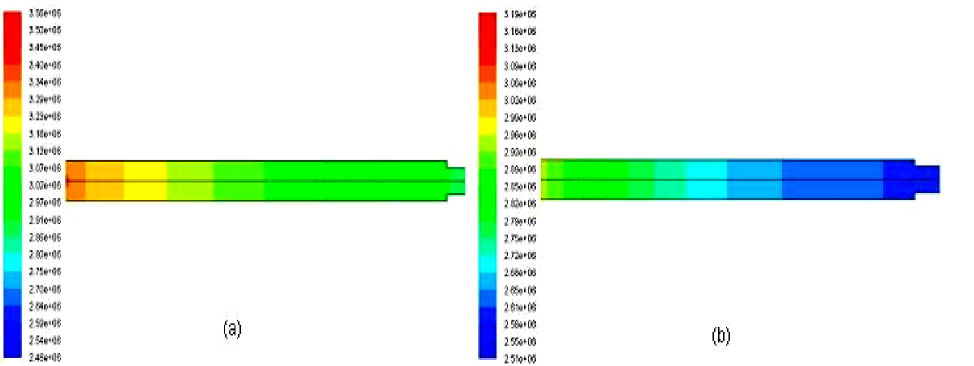


Figure 6. Instantaneous pressure variations in the regenerator (a) Thermal equilibrium model (b)

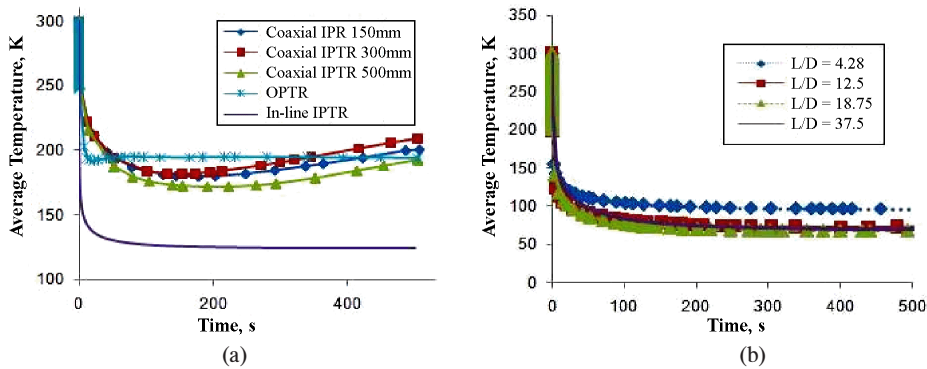


Figure 7. (a) Cooldown characteristics of different types of pulse tubes (b) Cool down characteristics with different length-to-diameter ratio.

temperature, while the minimum temperature reached by models with length-to-diameter ratio above 12.5 is almost the same. This phenomenon can be explained as follows:

It is possible to distinguish three important fluid zones in the pulse tube cooler. These are the cold gas zone near the cold heat exchanger, pulse tube gas central zone and the hot gas zone near the hot heat exchanger. Pulse tubes with smaller length to diameter ratio tend to even out the temperature gradient across the pulse tube because of the mixing of gases from the three zones and also due to axial heat conduction. This prevents the cold heat exchanger from attaining the lowest possible temperature. Although the larger length-to-diameter ratio decreases the axial conduction, it also increases the volume of pulse tube central gas zone. There is an optimum volume required to prevent mixing of cold and hot gas zones. This additional gas volume is not actively involved in the heat transfer processes and results in higher frictional dissipation thereby increasing the compressor work and decreasing the overall effectiveness of the pulse tube refrigerator. Thus it can be concluded that too long or too short pulse tubes are not desirable for practical applications.

The Effect of Finite Wall thickness Figure 8a shows the cooldown curve for pulse tube with length-to-diameter ratio of 18.75. The cycle-average temperature refers to that at the exit of the cold heat exchanger. The modeling of the porous zone is done with thermal equilibrium. The pulse tube model without wall takes only 200 seconds to reach 95% of the steady state temperature of 65 K while the model with wall takes almost 450 seconds to reach the steady state temperature of 130 K. The model with finitely thick wall represents the actual cool down taking place in pulse tube since

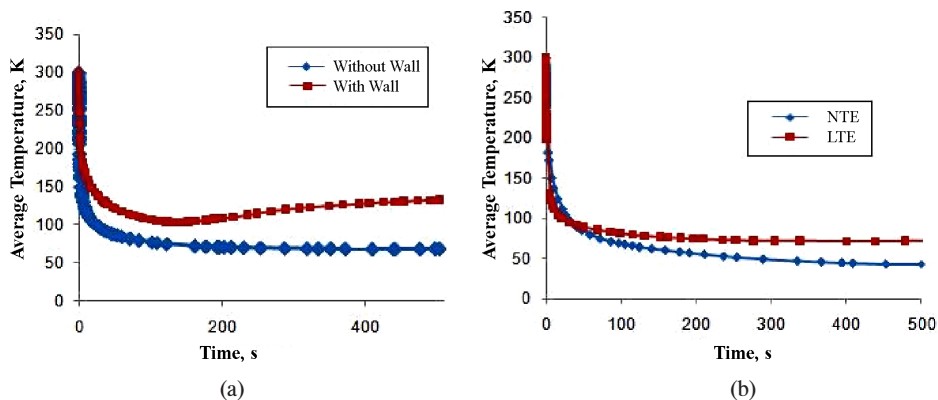


Figure 8. (a) Cooldown characteristics with wall and without wall (length-to-diameter ratio 18.75) (b) Cool down characteristics with thermal equilibrium and thermal non-equilibrium of porous zones (length-to-diameter ratio 12.5).

it captures the surface heat pumping process. The axial heat conduction is believed to be responsible for the higher cold heat exchanger temperature with the wall thickness taken into account.

The Effect of Local non-thermal equilibrium in Porous Zones Figure 8(b) presents the effect of introducing thermal non-equilibrium in the porous zones for pulse tube with length-to-diameter ratio of 25. The thermal equilibrium model exhibits rapid cooling followed by leveling off of the temperatures, while the thermal non-equilibrium model shows comparatively gradual cooling and stabilization of temperatures. The thermal non-equilibrium model takes longer time (above 400 seconds) for reaching the steady state while the thermal equilibrium model attains steady state much earlier, i.e., in about 200 seconds. The final temperature reached with thermal non-equilibrium model is lower than that of the thermal equilibrium model. It may be recalled that either model requires the use of pressure drop correlations in oscillating flow in porous zones. However, the thermal non-equilibrium model additionally requires the use of heat transfer correlations in oscillating flow, as mentioned earlier. The accuracy of the heat transfer correlations can have an effect on the accuracy of the results obtained for the thermal non-equilibrium case.

CONCLUSIONS

An improved approach, taking into account the complete set of conservation equations in axisymmetric coordinates, finite wall thickness and local non-thermal equilibrium, is adopted for modeling different types of pulse tube refrigerators. In view of this, the results obtained from the present model are more realistic as compared to the simplified analyses, like phasor and linear network, reported in the literature. The CFD analysis has shown that the in-line IPTR performs much better than coaxial IPTR and in-line OPTR. CFD analysis clearly reveals the multi dimensional flow and heat transfer effect at the component junctions. The inferior performance of in-line OPTR is due to the eddy formation near the orifice region. Optimization of length-to-diameter ratio for attaining minimum cold heat exchanger temperature is possible for a given pulse tube geometry by CFD analysis presented in this paper. The effect of axial conduction on the performance of pulse tube is analyzed by introducing finite wall thickness to all the components except the compressor. The oscillatory flow matrix-gas interactions are taken into account by introducing more realistic thermal non-equilibrium model for all the porous zones. The feasibility of the PTR modeling with CFD packages and the use of CFD packages as design tools should be weighed against the disadvantage of very large computing time, which, in the present case, is about one month CPU time per run.

ACKNOWLEDGMENTS

The authors gratefully acknowledge the help of the staff of the Super-computing Education and Research Centre (SERC) of the Indian Institute of Science, Bangalore, for running the FLUENT model. The authors express their sincere thanks to Prof. P.V. Desai and Prof. S.M. Ghiaasiaan of Georgia Institute of Technology, and Dr. J.S. Cha of The Aerospace Corporation for the helpful suggestions.

REFERENCES

1. Zhu Shaowei., Matsubara Yoichi., "Numerical method of inertance tube pulse tube refrigerator," *Cryogenics*, Vol.44, (2004), pp. 649-660.
2. Razani, A., Dodson, C., Flake, B., Roberts, T., "The effect of phase-shifting mechanism on energy and exergy flow in pulse tube refrigerators," *Advances in Cryogenic Engineering*, Vol.51-B, (2005), pp. 1572-1597.
3. Cha, J.S., Ghiaasiaan, S.M., Desai, P.V., Harvey, J.P., Kirkconnell, C.S., "Multi-dimensional flow effects in pulse tube refrigerators," *Cryogenics* Vol. 46, (2006) , pp. 658-665.
4. Flake, B., Razani, A., "Modeling pulse tube cryocoolers with CFD," *Advances in Cryogenic Engineering*, American Institute of Physics, Melville, NY, Vol.49, 2004 , pp. 1493-1499.
5. Harvey, J.P., "Oscillatory Compressible Flow and Heat Transfer in Porous Media-Application to Cryocooler Regenerators," Ph.D. Thesis, Georgia Institute of Technology, Atlanta, Ga, 2003.

6. Tanaka, M., Yamashita, I., Chisaka, F., "Flow and heat transfer characteristics of Stirling engine regenerator in an oscillating flow," *JSME International Journal*, Vol.33 (II), (1990) , pp. 283-289.
7. Imura, J., Shinoki, S., Sato, T., Iwata, N., Yamamoto, H., Yasohama, K., Ohashi, Y., Nomachi, H., Okumura, N., Nagaya, S., Tamada, T., Hirano, N., "Development of High Capacity Stirling Type Pulse Tube Cryocooler," *Physica C*, Vol. 463-465, (2007) ,pp.1369-1371.
8. Koh, J.C.Y., Fortini A., "Prediction of thermal conductivity and electrical resistivity of porous metallic materials," *Int. J. Heat Mass Transfer*, Vol.16, (1973) , pp.2013-2022.
9. Clearman, W.M., Cha, J.S., Ghiaasiaan, S.M., Kirkconnell, C.S., "Anisotropic steady-flow hydrodynamic parameters of microporous media applied to pulse tube and Stirling cryocooler regenerators," *Cryogenics*, Vol. 48, Issues: 3-4 (Mar.-Apr. 2008), pp. 112-121.